Characterization of near-wall turbulence in terms of equilibrium and periodic solutions

By Genta Kawahara †, Javier Jiménez ‡, Makoto Shiba ¶ AND Mark Simens ‖

Near-wall turbulence in the buffer region is qualitatively characterized in terms of recently-found nonlinear three-dimensional solutions to the incompressible Navier–Stokes equation for wall-bounded shear flows. Jiménez & Simens' (2001) traveling-wave solution for an autonomous wall flow, Nagata's (1990) steady and Kawahara & Kida's (2001) periodic solutions for a plane Couette flow are considered for characterization. These equilibrium and periodic solutions are classified into two families, of which one is dominated by streamwise vortices, and the other by streaks. The former family, which is composed of autonomous solutions, Nagata's upper-branch solutions and time-periodic solutions, is similar to fully-turbulent simulationss in the near-wall region.

1. Introduction

Since the famous 1883 experiments by Reynolds, wall-bounded turbulent flow has been one of the main subjects of turbulence research. The lack of a simple spatio-temporal characterization of turbulence has, however, impeded the elucidation of the structural and dynamical properties of near-wall turbulent flows.

Recently, several nonlinear equilibrium solutions of the three-dimensional Navier–Stokes equations have been obtained numerically for wall-bounded shear flows, such as plane Couette flow (Nagata 1990), plane Poiseuille flow (Toh & Itano 1999; Waleffe 2001), and an autonomous wall flow (Jiménez & Simens 2001). The equilibrium solutions of these systems exhibit a similar structure in physical space (see Waleffe 1998; Kawahara, Jiménez, Uhlmann & Pinelli 2002), which takes the form of wavy low-velocity streaks flanked by staggered streamwise vortices of alternating signs. These solutions are unstable at the Reynolds numbers where turbulence is observed, and they represent saddles in phase space, in the neighbourhood of which a turbulent state could spend a substantial fraction of time. Their structure closely resembles the spatially-coherent objects observed in the near-wall region of turbulent flows.

More recently Kawahara & Kida (2001) have numerically extracted a periodic saddle orbit embedded in low-Reynolds-number plane Couette turbulence, which well characterizes not only spatial but also temporal coherence of near-wall turbulence, i.e. a full regeneration cycle of low-velocity streaks and streamwise vortices. Besides, the mean velocity profile and the root-mean-square velocity fluctuations of plane Couette turbulence agree very well with the temporal averages of those of the periodic solution.

Of these solutions, those which are obtained as equilibrium and periodic solutions of the Navier–Stokes equations usually form parametric families, while those educed from turbulent flows have parameters which fall in definite ranges. The best-known case is

† Kyoto University
‡ Also at Universidad Politécnica de Madrid
¶ Ehime University
‖ Universidad Politécnica de Madrid

of course the spanwise-wavelength selection mechanism that results in the mean streak separation of $z^+ \approx 100$, but equally intriguing is the observed $x^+ \approx 300$ streamwise separation between vortex pairs within the same streak (Jiménez & Moin 1991). Although the similarities observed between the theoretical and educed structures are striking, and definitely suggest that they are related to each other and to self-sustaining wall turbulence, the exact nature of this relation is still unclear.

The main objective of this work is to clarify this relation. We shall put together several of the known equilibrium and periodic solutions for wall-bounded shear flows. Traveling-wave solutions for an autonomous wall flow (Jiménez & Simens 2001), steady (Nagata 1990) and periodic (Kawahara & Kida 2001) solutions for a plane Couette flow will be compared and checked against those of real near-wall turbulence.

The numerical methods used to recompute some of these solutions are described in section 2. Comparisons between the different equilibrium and periodic solutions are made in section 3, and their relation with fully-developed turbulence is discussed in section 4. Finally some conclusions are offered in section 5.

2. Equilibrium and periodic solutions

2.1. *Autonomous solutions*

The permanent solutions described below as 'autonomous' are computed using a slightly modified version of the numerical scheme described by Jiménez & Pinelli (1999) and by Jiménez & Simens (2001). The Navier-Stokes equations are integrated in the form of evolution equations for the wall-normal vorticity ω_y and for $\phi = \nabla^2 v$, using a pseudospectral code with Fourier expansions in the two wall-parallel directions and Chebychev polynomials in the wall-normal direction y, as in Kim, Moin & Moser (1987). At each time step the right-hand sides of the two evolution equations are multiplied by a damping mask $1 - \Delta t\, F(y)$, where

$$F(y) = 0 \quad \text{if} \quad y \le \delta_1, \qquad F(y) = 1/T \quad \text{if} \quad y \ge \delta_2. \tag{2.1}$$

The two limits of $F(y)$ are connected smoothly by a cubic spline. For the solutions used in this paper, $\delta_2 = 1.5\,\delta_1$. This mask can be interpreted as a linear dissipation for each of the two evolution variables, acting only above $y = \delta_1$. The equations being solved are, to numerical accuracy,

$$\partial_t \omega = N - F(y)\omega. \tag{2.2}$$

where ω stands for any of the two evolution variables, and N represents the full right-hand side of the Navier–Stokes equations. The evolution equations are not modified below the mask lower limit δ_1, but F is chosen large enough for all the vorticity fluctuations to be effectively damped above $y \approx (\delta_1 + \delta_2)/2$. Irrotational fluctuations are not affected, and the outer edge of the Navier–Stokes layer is bounded by a potential core which prevents the formation of viscous boundary layers at the mask boundary.

While the flows in Jiménez & Pinelli (1999) and in Jiménez & Simens (2001) were integrated at constant mass flux in a channel, the present computations were initially carried out at constant driving stress in a 'semi-infinite' domain. No-slip, impermeable boundary conditions were imposed at $y = 0$, and the velocities were matched to outer potential fluctuations extending to infinity from the edge of the computational domain, $y = h > \delta_2$, using the method introduced by Corral & Jiménez (1995). This driving mechanism is free from the complications of a 'second wall' across the potential layer, and in particular from the effect of a mean pressure gradient, and should in principle be

L_x^+	L_z^+	δ_1^+	U_c^+	u'^+_{max}	v'^+_{max}
167	180	38.4	13.2	2.54	0.592
151	180	42.0	13.2	2.51	0.578
167	180	42.0	12.8	2.59	0.598
188	180	42.0	12.6	2.71	0.615
188	180	45.6	12.4	2.84	0.612

TABLE 1. Parameters of the autonomous simulations used in the text. L_x and L_z are the box dimensions, U_c is the phase velocity, and u'_{max}, v'_{max} are the two parameters used below to characterize solutions.

preferable to simulations involving two-walled channels. The Reynolds shear stress, for example, is constant across the Navier-Stokes layer, instead of varying linearly across the channel and the only parameter in the problem is the Reynolds number δ_1^+. In this paper the superscript $^+$ is attached to wall variables that are normalized with the kinematic viscosity ν and the friction velocity u_τ. The driving mechanism was successfully used in Jiménez, Flores & García-Villalba (2001) to simulate autonomous wall flows in a large, but shallow, computational box.

In the present case however this driving mechanism failed to reproduce the simple solutions found by Jiménez & Simens (2001). The flow passed directly from fully-chaotic (minimal) turbulence to laminar decay, upon minor changes of the mask height or of the box dimensions.

It was therefore decided to reintroduce some pressure effects. The basic structure of the code is maintained, and in particular the driving mechanism for the mean flow is still a mean shear away from the wall, instead of an imposed mean pressure gradient. The mean velocity profile tends to linear, rather than to parabolic, away from the wall. The potential fluctuations in the masked region, however, instead of being defined as decaying at $y \to \infty$, are required to match a no-stress impermeable boundary at $y = H > h$. The vertical structure of the potential wall-normal velocity Fourier mode with streamwise and spanwise wavenumbers α and β is, for example, proportional to $\sinh[(\alpha^2+\beta^2)^{1/2}(y-H)]$, instead of to $\exp[-(\alpha^2+\beta^2)^{1/2}y]$. All the cases presented in this paper were computed with $H = 2h$ and with the viscosity adjusted so that $h^+ = 120$.

This modification introduces a fluctuating pressure gradient which maintains the instantaneous mass flow constant across the domain $(0, H)$. It was found to be sufficient to restore the existence of simple solutions, with a complex bifurcation structure which will be discussed elsewhere. The significance of this observation is not clear, although it is not surprising that the dynamical properties of constant-mass and constant-stress simulations should differ in such small computational domains. Here we only use solutions which behave like permanent waves. Their computational parameters are summarized in table 1, where L_x and L_z are the box dimensions, U_c is the phase velocity, and u'_{max}, v'_{max} are the two parameters used below to characterize solutions. Because of the presence of a required fluctuation of spatially-constant pressure gradient, these flows are classified below as part of the Poiseuille family.

2.2. *Plane Couette solutions*

Here, Nagata's (1990) steady solutions of the incompressible Navier–Stokes equation for a plane Couette flow are recomputed by the Newton–Raphson method (see Shiba 2001 for detailed numerical procedures). It is well known that a laminar plane Couette flow is lin-

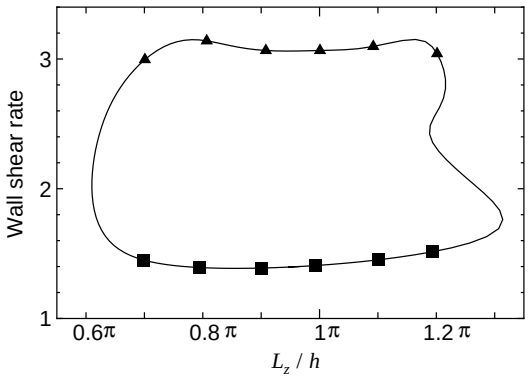

FIGURE 1. The dimensionless wall shear rate for Nagata's solution versus the spanwise period L_z. The Reynolds number Re and the streamwise period L_x are fixed as $Re = 400$ and $L_x = 2\pi h$.

early stable for all finite Reynolds numbers. Nagata's upper and lower solution branches appear subcritically at $Re \approx 125$ from saddle–node bifurcation, where $Re = Uh/\nu$ is the Reynolds number, U and h denoting half the difference of the two wall velocities and half the wall separation, respectively. In general, the upper-branch (or lower-branch) solutions generated from the bifurcation have a larger (or smaller) deviation from a laminar state.

As in Ehrenstein & Koch (1991), the flow is decomposed into a laminar part and a deviation from it, and then the latter is obtained numerically by solving steady nonlinear equations for the streamwise velocity $u_0(y)$ averaged over a plane parallel to the wall, for the wall-normal vorticity $\omega_y(x, y, z)$, and for the Laplacian of the wall-normal velocity, $\phi = \nabla^2 v(x, y, z)$. The solutions are assumed to be spatially periodic in the wall-parallel directions, and they are expressed as double Fourier expansions in these two directions. In the expansion with respect to the wall-normal dimensionless coordinate y^* $(= y/h)$, where the plane $y = 0$ is now the midplane of the channel, we use the two kinds of modified Chebychev polynomials as

$$(1 - y^{*2})\, T_l(y^*) \quad \text{for } u_0 \text{ and } \omega_y \tag{2.3}$$

and

$$(1 - y^{*2})^2\, T_l(y^*) \quad \text{for } v, \tag{2.4}$$

respectively, to satisfy the wall boundary conditions

$$u_0 = \omega_y = v = \frac{\partial v}{\partial y} = 0 \quad \text{at } y^* = \pm 1, \tag{2.5}$$

where $T_l(y^*)$ is the lth-order Chebychev polinomial. The collocation method with grid points $y^* = \cos[m\pi/(M+1)]$, $(m = 1, 2, \cdots, M)$ is used to construct a system of quadratic equations for the Fourier–Chebychev–Fourier coefficients, which is solved by the Newton–Raphson method. The arc-length method (see Ehrenstein & Koch 1991) is applied to track the nonlinear solutions, with the parameters, i.e. Re, L_x or L_z, being changed independently.

The Nagata solutions are known to have two spatial symmetries (see Nagata 1986, 1988, 1990): (i) the reflection with respect to the plane of $z = 0$ and a streamwise shift by a half period $L_x/2$

$$(u, v, w)(x, y, z) = (u, v, -w)(x + L_x/2, y, -z), \tag{2.6}$$

L_x^+	L_z^+	Re_τ	u'^+_{max}	v'^+_{max}
217	76.2	34.6	2.79	0.887
223	89.8	35.4	2.84	0.892
220	99.9	35.0	2.84	0.840
220	110	35.0	2.85	0.768
221	121	35.2	2.97	0.674
219	132	34.9	3.42	0.534

TABLE 2. Parameters of Nagata's upper-branch solutions represented by ▲ in figure 1. $Re_\tau = u_\tau h/\nu$ is the Reynolds number or half the wall separation in wall units.

L_x^+	L_z^+	Re_τ	u'^+_{max}	v'^+_{max}
151	53.5	24.1	3.20	0.302
148	58.9	23.6	3.70	0.230
156	66.7	23.6	4.16	0.194
149	74.0	23.7	4.50	0.179
151	83.3	24.1	4.85	0.170
155	92.2	24.6	5.09	0.169

TABLE 3. Same as table 2 but for the lower-branch solutions represented by ■ in figure 1.

L_x^+	L_z^+	Re_τ	T_p^+	$\overline{u'}^+_{max}$	$\overline{v'}^+_{max}$
190	130	34.4	188	3.18	0.741
154	105	27.9	299	4.62	0.231

TABLE 4. Parameters of two kinds of periodic solutions (Kawahara & Kida 2001). T_p^+ stands for the time period of the solution. $\overline{u'}^+_{max}$ and $\overline{v'}^+_{max}$ are the time averages of u'^+_{max} and v'^+_{max}.

and (ii) the 180° rotation around the line $x = y = 0$ and a spanwise shift by a half period $L_z/2$

$$(u, v, w)(x, y, z) = (-u, -v, w)(-x, -y, z + L_z/2), \tag{2.7}$$

where u and w are the streamwise and the spanwise components of the velocity deviation. Note that these two symmetries were observed to appear approximately in minimal plane Couette turbulence (Hamilton, Kim & Waleffe 1995) as well, without being imposed on the flow (Coughlin, Jiménez & Moser 1994; Kawahara & Kida 2001). These symmetries have also been imposed on the time-periodic solutions below.

Figure 1 shows the dimensionless wall shear rate, $\mathrm{d}u_0/\mathrm{d}y|_{y=\pm h}/(U/h) + 1$, averaged over the wall as a function of the spanwise period of the solution, L_z. The symmetry (2.7) implies that the averaged velocity gradients on the lower and upper walls are equal to each other. The Reynolds number Re and the streamwise period L_x have been fixed as $Re = 400$ and $L_x = 2\pi h$. Both the upper and the lower branches have a higher shear rate compared with that for a laminar state, i.e. unity. The computational parameters for the upper and the lower solutions, which will be compared with the autonomous and periodic solutions or with the turbulent solutions, are summarized in tables 2 and 3 respectively.

The two kinds of time-periodic solutions for a plane Couette flow are taken from Kawa-

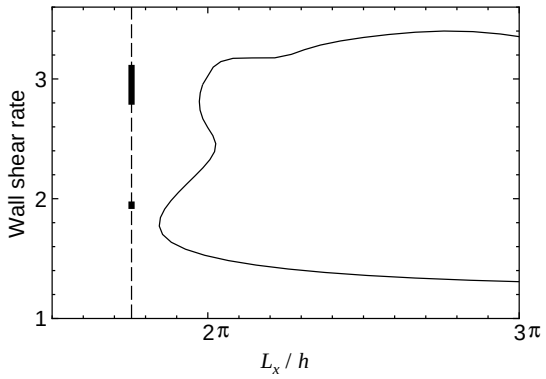

FIGURE 2. The dimensionless wall shear rate for the Nagata's solution versus the relatively small streamwise period L_x. The Reynolds number Re and the spanwise period L_z are fixed as $Re = 400$ and $L_z = 1.2\pi h$. The dashed vertical line denotes the period of $L_x = 1.755\pi h$, for which the two kinds of time-periodic solutions were found by Kawahara & Kida (2001) at the same values of Re and L_z. The upper long (or lower short) thick line on the vertical represents the wall shear variation of the time-periodic solution with the period $T_p^+ = 188$ (or $T_p^+ = 299$).

hara & Kida (2001) to be compared with the other solutions. Their periodic solutions have been obtained for the conditions $Re = 400$, $L_x = 1.755\pi h$ and $L_z = 1.2\pi h$, which are essentially the same as those of minimal plane Couette turbulence in Hamilton, Kim & Waleffe (1995). The parameters for the periodic solutions are summarized in table 4. As can be seen from figure 2, there is no Nagata steady solution at the conditions, for which time-periodic solutions were observed in Kawahara & Kida (2001). The wall shear rate of the periodic solution with period $T_p^+ = 188$ is roughly the same as that of Nagata's upper branch. The other periodic solution with $T_p^+ = 299$ has a lower wall shear rate, close to Nagata's lower branch. Hereafter, the former solution is referred to as the 'upper' periodic solution, while the latter is called the 'lower' periodic solution. The upper solution exhibits a full regeneration cycle of near-wall coherent structures, and also well represents the low-order turbulence statistics of a minimal plane Couette flow (Kawahara & Kida 2001).

3. Classification of solutions

In this section, we compare the equilibrium and periodic solutions described in the preceding section. The streamwise and wall-normal rms velocities, u' and v', for the upper solutions as well as for the autonomous solutions, are shown in figure 3, while those for the lower solutions are shown in figure 4. It can be seen that the rms velocities of the autonomous solution, Nagata's upper-branch solution and the upper-periodic solution are roughly consistent, but that they are very different from the lower-branch and lower-periodic solutions. The profiles of the autonomous and upper-periodic solutions in figure 3 seem to be qualitatively similar to those of near-wall turbulence, and the similarity will be discussed in the next section. The lower solutions, on the other hand, have stronger u'^+ and weaker v'^+, which implies that they are dominated by streaks rather than streamwise vortices and so are in a relatively quiescent state.

Since significant differences in the rms velocities are observed between the solutions, we next use the maximum rms velocities in the streamwise and wall-normal directions, u'_{max} and v'_{max}, to characterize them. It turns out from figure 5 that all the solutions are clas-

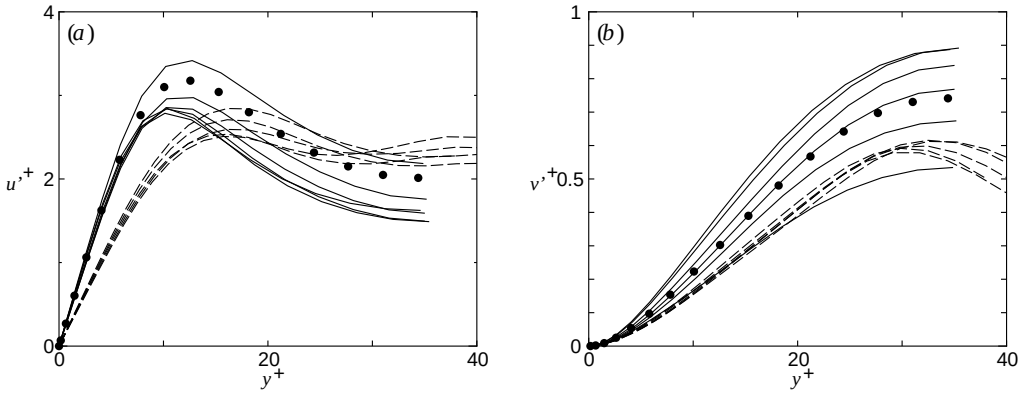

FIGURE 3. Rms velocities for the autonomous solutions, Nagata's upper branch, and the upper cycle versus y^+. (a) The streamwise component. (b) The wall-normal component. - - - - , the autonomous solutions from table 1; ——— , Nagata's upper-branch solutions from table 2; • , the upper cycle with the period $T_p^+ = 188$ from table 4.

sified into two families. One of them is the vortex-dominated family, which is represented by larger v'^+_{max}, and is composed of the autonomous, upper-branch and upper-periodic solutions. The other is the streak-dominated family, which is composed of Nagata's lower branch and the lower periodic solution. The same separation into families is found if we replace v'_{max} by the maximum of the streamwise rms vorticity ω'_x (not shown here). This means that the former family is actually dominated by streamwise vortices. In this figure we have added two of Nagata's solutions for different values of Re and L_x. They have been tracked by changing L_z for fixed Re and L_x in the same way as in figure 1. The open circles and diamonds represent the upper and lower branches for $Re = 600$ and $L_x = 2\pi h$. The solid circles and diamonds represent the upper and lower branches for $Re = 400$ and $L_x = 3\pi h$. Since the separation into two branches persists even when the parameters are changed, we can assume that it is an intrinsic property of the solution.

The simple solutions discussed here have distinct natures, e.g. either (i) autonomous or Couette flow, and (ii) steady, traveling-wave, or periodic. It is remarkable that all the solutions are classified into just two families.

Let us further compare the autonomous and upper-cycle solutions, which have been classified into the same family. Figure 6 shows these solutions on the plane whose coordinates are the total turbulent production and dissipation rates, P^+ and D^+, which are respectively defined as the integrals of the turbulent production and dissipation with respect to y^+ up to $y^+ = h^+$ (up to δ_1^+ in the autonomous case). Note that the autonomous solutions, though in equilibrium, are not in energy balance because of the presence of explicit filtering (2.1). Since the filter is responsible for part of the energy dissipation, the production exceeds the dissipation in the autonomous flows themselves. The autonomous solutions are roughly aligned along the periodic orbit in the production phase in which $P^+ > D^+$. In figure 7, we compare the spanwise rms velocity for the autonomous solutions with that averaged over one whole period for the periodic solution, as well as with that averaged only in the production (or dissipation) phase, $P^+ > D^+$ (or $P^+ < D^+$). It is clear that the autonomous solutions are closer to the time average of the upper cycle solution in the production phase than to the average over the whole period. The striking difference in w' between the production and the dissipation phases is also quite interesting. No significant difference in the other two components of rms velocities is observed.

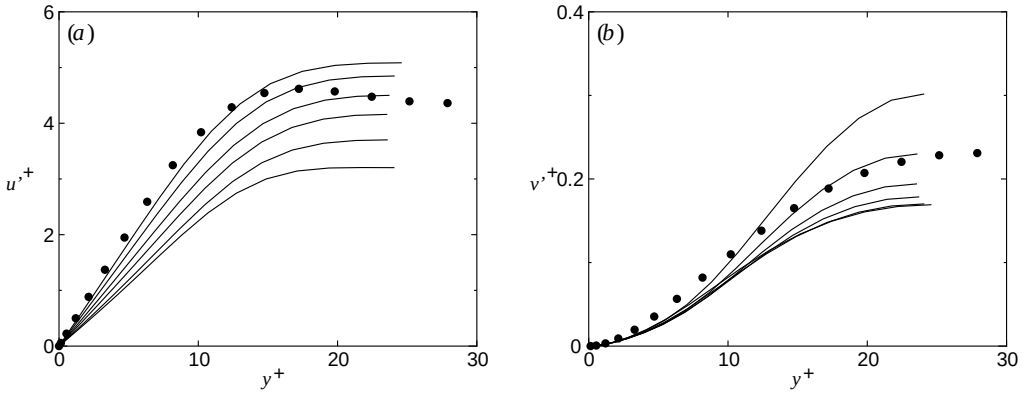

FIGURE 4. Rms velocities for Nagata's lower branch and the lower cycle against y^+. (a) The streamwise component. (b) The wall-normal component. ——— , Nagata's lower-branch solutions from table 2; • , the lower cycle with the period $T_p^+ = 299$ from table 4.

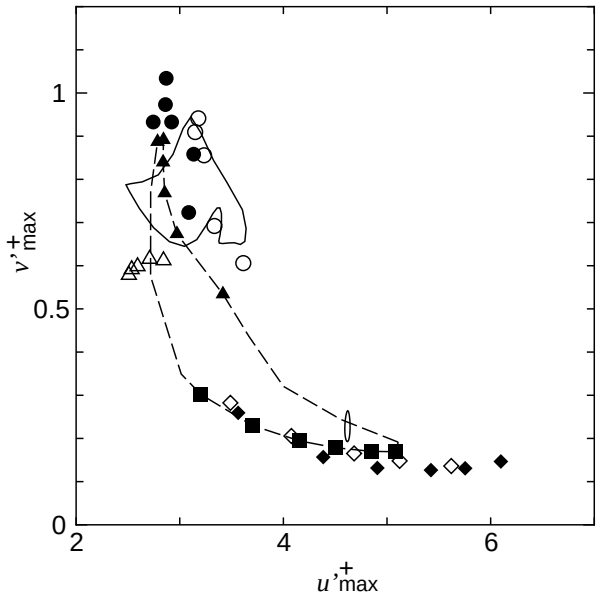

FIGURE 5. Classification into upper and lower solutions in terms of the maximum streamwise and wall-normal rms velocities, u'_{max} and v'_{max}. The solid large and small loops represent the upper and lower periodic solutions with $T_p^+ = 188$ and 299 in table 4, respectively. The dashed loop represents the Nagata steady solution for $Re = 400$ and $L_x = 2\pi h$ in figure 1. △, the autonomous solutions from table 1; ▲ , Nagata's upper-branch solutions from table 2; • , Nagata's upper-branch solutions for $Re = 400$ and $L_x = 3\pi h$; ○ , Nagata's upper-branch solutions for $Re = 600$ and $L_x = 2\pi h$. ■ , Nagata's lower-branch solutions from table 3; ♦ , Nagata's upper-branch solutions for $Re = 400$ and $L_x = 3\pi h$; ◇ , Nagata's lower-branch solutions for $Re = 600$ and $L_x = 2\pi h$.

Enhancement of the spanwise fluid motion is considered to be closely related with the sinuous instability of streaks (Kawahara, Jiménez, Uhlmann & Pinelli 2002).

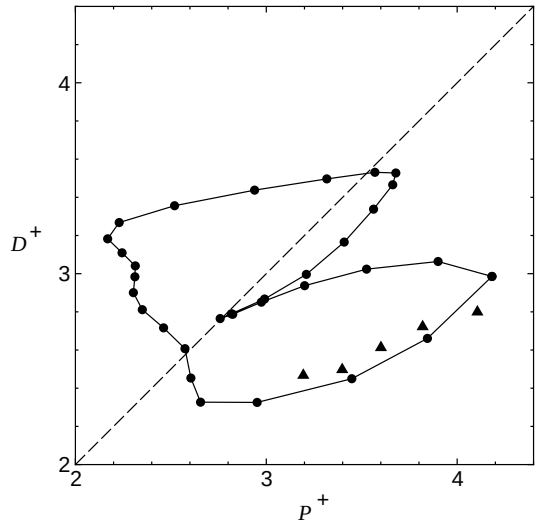

FIGURE 6. Total turbulent production and dissipation rates for the autonomous and the upper periodic solutions. ▲ , autonomous solutions from table 1; —●— , the upper periodic solution with $T_p^+ = 188$ in table 4. The production and dissipation are in balance on the dashed diagonal.

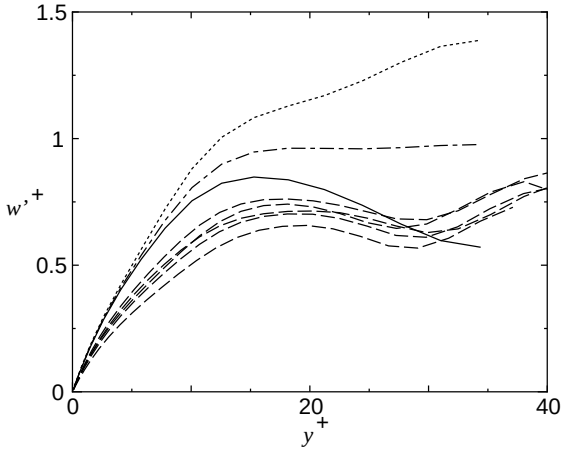

FIGURE 7. Spanwise rms velocities for the autonomous and the upper periodic solutions against y^+. - - - - , the autonomous solutions from table 1; —·— , the whole time average of the upper periodic solution with $T_p^+ = 188$ in table 4. ——— , the time average of the upper periodic solution in a production phase $P^+ > D^+$; ····· , the time average of the upper periodic solution in a dissipation phase $P^+ < D^+$.

4. Comparison with turbulent flows

After the classification in the previous section of the different simple solutions of the Navier–Stokes equations, it is interesting to inquire about their relation with fully developed turbulence in channels with large computational boxes (del Álamo & Jiménez 2001). We will use for that purpose the same two quantities u'_{max}, v'_{max} used above for the characterization of the simple solutions although, to make them comparable in both cases, we will refer them to boxes of comparable sizes. Thus, when computing the statistics of

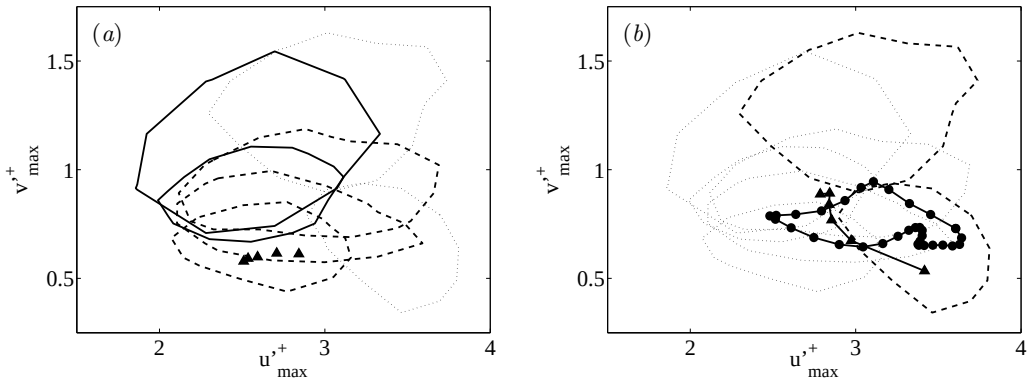

FIGURE 8. Comparison between turbulent and simple solutions. (a) Poiseuille flows. ——— , full channels from del Álamo & Jiménez (2001). The statistics are taken over sub-boxes of size $L_x^+ \times L_z^+ \approx 380 \times 180$. $Re_\tau = 550$, 180, decreasing from top to bottom; - - - - , minimal channels in boxes of approximately the same size as above. From top to bottom, $Re_\tau = 180$, 120, 85; ····· , Couette flows from (b), included for comparison; ▲ , autonomous permanent waves from table 1. (b) Couette flows. - - - - , minimal flows, $L_x^+ \times L_z^+ \approx 350 \times 150$. From top to bottom, $Re_\tau = 115$, 34. ····· , Poiseuille flows in (a); —●— , the upper cycle with $T_p^+ = 188$ from table 4; —▲— , the Nagata's upper branch from table 2.

full-sized turbulent channels, which have boxes of the order of $L_x^+ \times L_z^+ \approx 10,000 \times 5,000$, we will divide each wall of the large box into sub-boxes of size comparable to the wavelengths of the simple solutions, and the rms velocity fluctuations computed over those sub-boxes are used for the comparison.

Each sub-box is characterized by its maximum rms intensities, and the values for different sub-boxes and for different times are summarized as a joint probability density function of the two quantities. Figure 8 shows probability isolines containing 75% of the samples for each flow, compared with the single points characterizing the instantaneous values of the different upper-branch solutions. It is clear that the p.d.f.s of the full flows converge towards the simple waves as the Reynolds number decreases. Both in the Poiseuille flows in figure 8(a) and in the Couette flows in figure 8(b), the lowest Reynolds number used for the turbulent simulations is very close to the minimum value below which turbulence cannot be sustained.

It is interesting that full-sized and minimal Poiseuille flows have slightly different behaviour as the Reynolds number increases, although this may not be too significant, because the statistics are fairly sensitive to the size of the box over which they are compiled. The scatter in u'_{max} increases markedly as the box in made narrower, clearly because the samples are taken over smaller pieces of the same large streaks. The same variability does not extend to v'_{max}, probably because the scale of the v features is always smaller than the sampling boxes being used (del Álamo & Jiménez 2001). Note also that Couette and Poiseuille flows diverge at low Reynolds numbers, which is not surprising since the interactions between the two walls are substantial in that limit, but that their statistics tend to converge at higher Reynolds numbers.

Since v' peaks fairly far from the wall, the maxima in the higher-Reynolds number channel in figure 8(a) were computed only for the layer below $y^+ = 180$, despite which the maximum wall-normal velocity increases with Re_τ. Similar results are obtained by using ω'_x, instead of v', to characterize the strength of the vortices, which supports the conclusion that the vortices get stronger. This is probably independent of any interaction

with the external flow, since Jiménez & Pinelli (1999) observed that the peak vorticity fluctuations in minimal channels increased with Reynolds numbers in the range $Re_\tau = 200 - 600$, even if there was essentially no outer flow in those cases.

Note that lower-branch solutions have not been included in figure 8. Although Kawahara & Kida (2001) found that minimal Couette flow occasionally visits solutions in that branch and then becomes strongly turbulent, the same could not be confirmed here for other cases, and may be a peculiarity of flows on the verge of relaminarization.

5. Conclusions

We have shown that several known simple solutions to the Navier-Stokes equations, particularly those which correspond to permanent waves and to limit cycles in autonomous flows (Jiménez & Simens 2001), and Couette flows, can be classified into upper- and lower-branch families which agree fairly well with the corresponding branches of the Couette waves found by Nagata (1990). The velocity statistics within each branch are reasonably consistent, even though the base flows are quite different.

Although Kawahara & Kida (2001) found that minimal Couette turbulence intermittently visits the lower-branch solutions, the same does not seem to be true in flows at somewhat higher Reynolds numbers, or in larger boxes, although occasional excursions cannot be ruled out. This could be interpreted to mean that the lower branch, which should be the saddle point which Toh & Itano (1999), Itano & Toh (2001) and Kawahara & Kida (2001) found to be involved in the transition to fully turbulent states, represents an occasional tendency of minimal turbulence to relaminarize and retransition, but that these events are not allowed at higher Reynolds numbers, or in larger boxes, because of the higher level of ambient perturbations.

Fully-turbulent flows, when analyzed over sub-boxes of size consistent with the wavelengths of the permanent waves, have been shown to tend to the upper-branch solutions as the Reynolds number decreases, both in Poiseuille and in Couette flows. A reasonable interpretation is therefore that the permanent waves and cycles in that branch embody the nonlinear regeneration cycle of near-wall turbulence that has been described in the past by many investigators.

Waleffe (1998, 2001) also reported the structural similarities of his upper-branch equilibrium states with near-wall turbulence, although he presented no statistics. Because we were not able to reproduce his solutions within the time of the summer school, they are not included in the present comparison.

6. Acknowledgements

We are grateful to Professor M. Nagata for reading an early version of the manuscript. G.K. and M. Shiba appreciate helpful discussions with Professor S. Yanase in the development of a numerical code for an equilibrium solution. This work was supported in part by a Grant-in-Aid for Scientific Research (C) from Japan Society for the Promotion of Science, by the Spanish CICYT contract BFM2000-1468 and by ONR grant N0014-00-1-0146. M. Simens was supported in part by a fellowship from the TMR Intermittency network of the EC.

REFERENCES

Corral, R. & Jiménez, J. 1995 Fourier/Chebyshev methods for the incompressible Navier Stokes equations in infinite domains, *J. Comput. Phys.* **121**, 261–270.

Coughlin, K., Jiménez, J. & Moser, R. 1994 Instability of streamwise vortices in plane channel flows. *Proc. 1994 Summer Program*, Center for Turbulence Research, NASA Ames/Stanford Univ., 229-244.

Del Álamo, J.C. & Jiménez, J. 2001 Direct numerical simulation of the very-large anisotropic scales in a turbulent channel. *Annual Research Briefs*, Center for Turbulence Research, NASA Ames/Stanford Univ., 329–342.

Ehrenstein, U. & Koch, W. 1991 Three-dimensional wavelike equilibrium states in plane Poiseuille flow. *J. Fluid Mech.* **228**, 111–148.

Hamilton, J.M., Kim, J. & Waleffe, F. 1995 Regeneration mechanisms of near-wall turbulence structures. *J. Fluid Mech.* **287**, 317–348.

Itano, T. & Toh, S. 2001 The dynamics of bursting process in wall turbulence. *J. Phys. Soc. Jpn.* **70**, 701–714.

Jiménez, J., Flores, O. & García-Villalba, M. 2001 The large scale organization of autonomous turbulent walls, *Annual Research Briefs*, Center for Turbulence Research, NASA Ames/Stanford Univ., 317–329.

Jiménez, J. & Moin, P. 1991 The minimal flow unit in near wall turbulence. *J. Fluid Mech.* **225**, 221–240.

Jiménez, J. & Pinelli A. 1999 The autonomous cycle of near wall turbulence, *J. Fluid Mech.* **389**, 335–359.

Jiménez, J. & Simens, M.P. 2001 Low-dimensional dynamics in a turbulent wall, *J. Fluid Mech.* **435**, 81–91.

Kawahara, G., Jiménez, J., Uhlmann, M. & Pinelli, A. 2002 Linear instability of a corrugated vortex sheet – a model for streak instability. Submitted to *J. Fluid Mech.*

Kawahara, G. & Kida, S. 2001 Periodic motion embedded in plane Couette turbulence: regeneration cycle and burst. *J. Fluid Mech.* **449**, 291–300.

Kim, J., Moin, P. & Moser, R. 1987 Turbulence statistics in fully developed channel flow at low Reynolds number. *J. Fluid Mech.* **177**, 133–166.

Nagata, M. 1986 Bifurcations in Couette flow between almost corotating cylinders. *J. Fluid Mech.* **169**, 229–250.

Nagata, M. 1988 On wavy instabilities of the Taylor-vortex flow between corotating cylinders. *J. Fluid Mech.* **188**, 585–598.

Nagata, M. 1990 Three-dimensional finite-amplitude solutions in plane Couette flow: bifurcation from infinity. *J. Fluid Mech.* **217**, 519–527.

Shiba, M. 2001 Equiliburium and turbulent solutions for a wall-bounded shear flow. *Master's thesis*, Ehime Univ. (in Japanese).

Toh, S. & Itano, T. 1999 Low-dimensional dynamics embedded in a plane Poiseuille flow turbulence. Traveling-wave solution is a saddle point? preprint. physics/9905012.

Waleffe, F. 1998 Three-dimensional coherent states in plane shear flows. *Phys. Rev. Letters* **81**, 4140–4143.

Waleffe, F. 2001 Exact coherent structures in channel flow. *J. Fluid Mech.* **435**, 93–102.